Electronic Supplementary Material (ESI) for Journal of Materials Chemistry A.

Thermodynamically favored stable hydrogen storage reversibility of $NaBH_4$ inside of bimetallic nanoporous carbon nanosheets

Wei Chen[a], Shunlong Ju[a], Yahui Sun[a], Tianren Zhang[b], Juan Wang[b], Jikai Ye[a], Guanglin Xia[a], Xuebin Yu*[a]*

Department of Materials Science, Fudan University, Shanghai 200433, China.
Zhejiang Tianneng Battery Co., Ltd., Changxing 313100, Zhejiang, China.
*E-mail: xiaguanglin@fudan.edu.cn (G. L. Xia), yuxuebin@fudan.edu.cn (X. B. Yu)

Experimental

Chemicals: $Ni(NO_3)_2 \cdot 6H_2O$, $Co(NO_3)_2 \cdot 6H_2O$, terephthalic acid (PTA), and dimethoxyethane (DME) were purchased from Aladdin Industrial Corporation. N, N-dimethylformamide (DMF) and ethanol were purchased from Sinopharm Chemical reagent Co., Ltd. Triethylamine (TEA) was purchased from Macklin Biochemical Co., Ltd. $NaBH_4$ was purchased from Sigma-Aldrich. All chemicals were used directly without further purification.

Synthesis of ultrathin NiCo-MOFs nanosheets (NiCo-MOFs): The preparation process of ultrathin NiCo-MOFs nanosheets was modified according to the previously published method.[S1, S2] In a typical synthesis procedure, 0.75 mmol $Ni(NO_3)_2 \cdot 6H_2O$, 0.75 mmol $Co(NO_3)_2 \cdot 6H_2O$ and 1.5 mmol PTA were dissolved in the mixed solvent mixture, containing 4 mL of ethanol, 4 mL of water and 64 mL of DMF. Subsequently, 1.6 mL TEA was quickly injected into the solution. After that, the mixture was stirred for 5 min to obtain a uniform colloidal suspension which was then continuously ultrasonicated for 8 h at room temperature. After washing with ethanol for 3 times, the as-obtained product was dispersed in water and ultrasonicated for 30 min. Finally, the obtained aqueous dispersion was subjected to freeze-drying for 72 h to obtain NiCo-MOFs.

Synthesis of bimetallic (NiCo) nanoporous carbon nanosheets (NiCo-NC): The NiCo-NC was prepared by the annealing of thus-obtained NiCo-MOFs at elevated temperature. Briefly, the as-prepared NiCo-MOFs was carbonized at 900 ℃ in a tube furnace for 1 h with a heating rate of 2 ℃ min^{-1} under Ar atmosphere. After cooling to room temperature, the black powers collected were collected and denoted as NiCo-NC.

Synthesis of $NaBH_4$@NiCo-NC: The synthesis of $NaBH_4$@NiCo-NC was realized according to the solution infiltration method. Typically, 50 mg of $NaBH_4$ was dissolved in 25 mL DME and stirred for 2h. Subsequently, 50 mg of NiCo-NC was added into the sol and the thus-obtained mixture was ultrasonically treated for 1 h to achieve the

homogeneous contact between $NaBH_4$ and NiCo-NC. The suspension was finally dried at 80 ℃ under vacuum for 12 h to remove the solvent to obtain $NaBH_4$@NiCo-NC.

Synthesis of nanoporous carbon nanosheets (NC): NC was prepared by etching NiCo from NiCo-NC. Certain amount of NiCo-NC was dispersed in 8 mol L^{-1} HCl solution and ultrasonicated for 1 h, followed by stirring for another 24 h. The product was washed with water for 4 times and dried in a drying oven at 80 ℃ for 12 h. The thus-obtained powder was denoted as NC.

Synthesis of ball-milled samples: The ball-milled composite of $NaBH_4$ and NiCo-NC (denoted as $NaBH_4$/NiCo-NC) was prepared by ball milling the mixture of $NaBH_4$ and NiCo-NC with a weight ratio of 1:1 at 300 rpm for 2 h on a planetary ball mill (QM-3SP4, Nanjing Nanda Instrument Plant). The ball-to-powder ratio was approximately 50:1.

Characterization

The hydrogen absorption and desorption performance of materials were quantitatively determined using a high-pressure gas sorption apparatus (HPSA-auto). Isothermal dehydrogenation measurements were conducted at several constant temperatures (*i.e.* 380 ℃, 400 ℃, 420 ℃, and 440 ℃) under static vacuum for 6 h. In the term of cycling hydrogen storage tests, the as-prepared materials were heated to 400 ℃ rapidly and hold for 6 h with an initial pressure lower than 0.001 bar, and the rehydrogenation of the dehydrogenated products was performed under a hydrogen pressure of 60 bar at 350 ℃ for 10 h.

Morphologies of the materials were observed by scanning electron microscopy (SEM, JEOL 7500FA) and transmission electron microscopy (TEM, JEOL JEM-2100F), while TEM-associated energy-dispersive X-ray spectroscopy (EDS) was used for elemental analysis. Phase compositions of the materials were identified by X-ray diffraction (XRD; D8 advance, Bruker AXS) with Cu Kα radiation at 50 kV and 30 mA. In order to avoid any possible oxidation during XRD measurement, all materials were pre-sealed on sample stages with scotch tape in an Ar-filled glovebox. Mass spectrometry (MS) was conducted using a mass spectrometer (HIDEN, QIC-20) from

room temperature to 600 ℃ with a heating rate of 3 ℃ min^{-1} under Ar flow. The signals at m/e = 2 and 27 were recorded in order to detect H_2 and B_2H_6. Chemical bonds in the materials were examined by Fourier transform infrared spectroscopy (FT-IR, Bruker Tensor 27). X-ray photoelectron spectroscopy (XPS) was carried out on a Thermo Scientific K-Alpha+ with Al X-ray radiation source.

DFT calculations

Density functional theory (DFT) calculations were carried out using projector-augmented wave (PAW) method as implemented in Vienna ab initio simulation package (VASP).[S3-S5] A generalized gradient approximation (GGA) of Perdew-Burke-Ernzerhof (PBE) functional was employed to describe the exchange-correlation interaction.[S6] The DFT-D3 method was also adopted to evaluate the van der Waals interactions.[S7] In all calculations, the energy cutoff was set as 500 eV, and Gamma centered k-points mesh with mesh point spacing less than 0.05 $Å^{-1}$ were applied. The structures were relaxed until the forces and total energy on all atoms were converged to less than 0.05 eV $Å^{-1}$ and 1×10^{-5} eV. To evaluate the difficulty of various re-/dehydrogenation reactions thermodynamically, the Gibbs free energy change (ΔG) was calculated as follows,

$$\Delta G = \sum G_{product} - \sum G_{reactant}$$

where $G_{product}$ and $G_{reactant}$ are the total energy of every product and reactant in the re-/dehydrogenation reaction formula, respectively. A reaction with lower ΔG is more likely to occur thermodynamically.

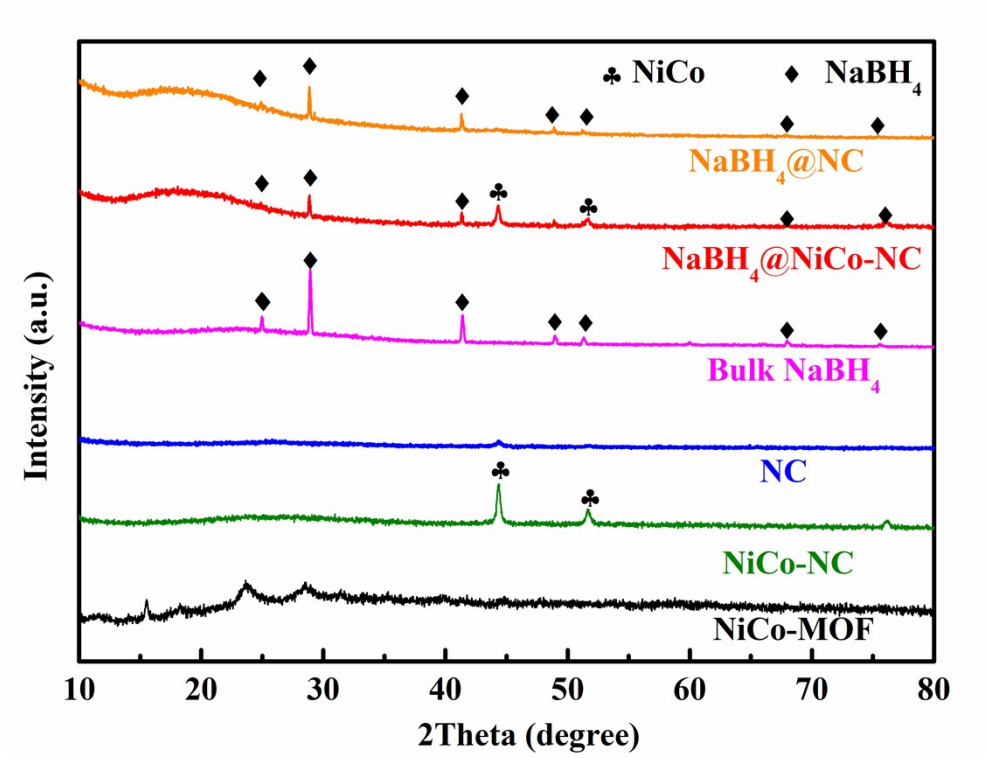

Figure S1. XRD patterns of the as-synthesized samples.

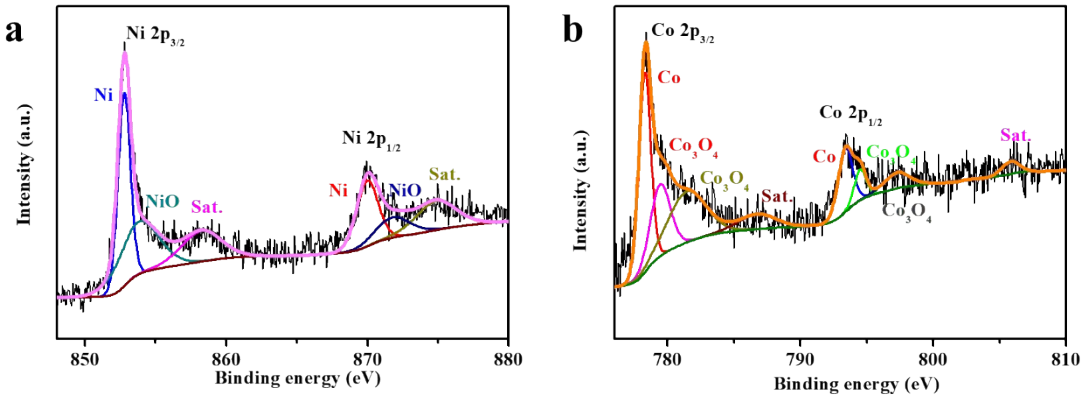

Figure S2. High-resolution Ni 2p (a) and Co 2p (b) XPS spectra of NiCo-NC.

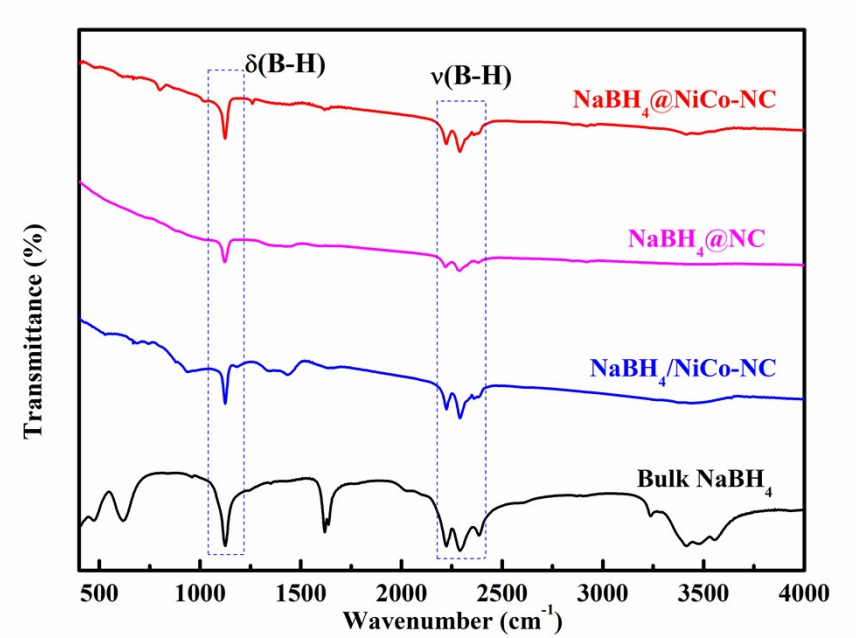

Figure S3. FTIR spectra of the as-prepared samples.

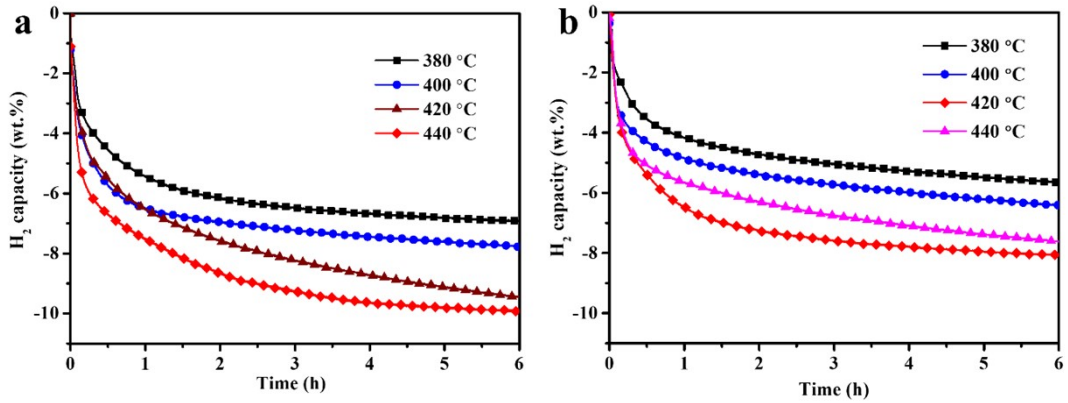

Figure S4. The isothermal dehydrogenation kinetics of (a) $NaBH_4$@NC and (b) $NaBH_4$/NiCo-NC at various temperatures.

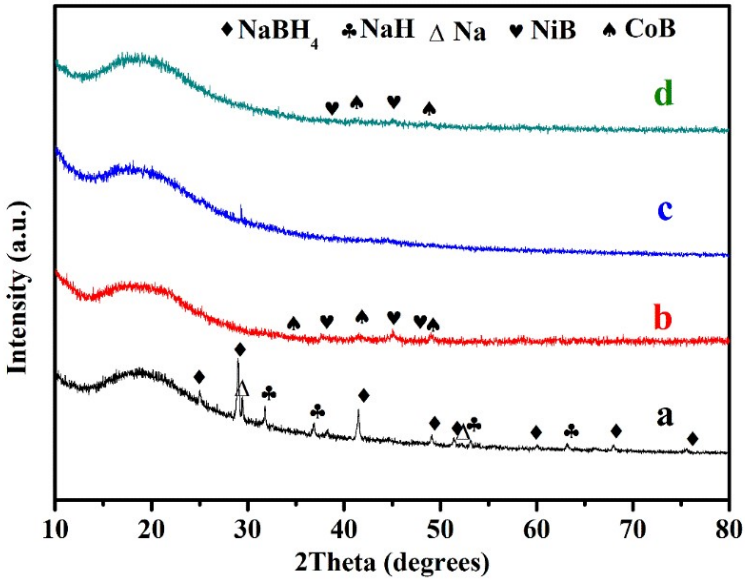

Figure S5. XRD patterns of the dehydrogenation products of (a) bulk $NaBH_4$, (b) $NaBH_4$/NiCo-NC, (c) $NaBH_4$@NC and (d) $NaBH_4$@NiCo-NC.

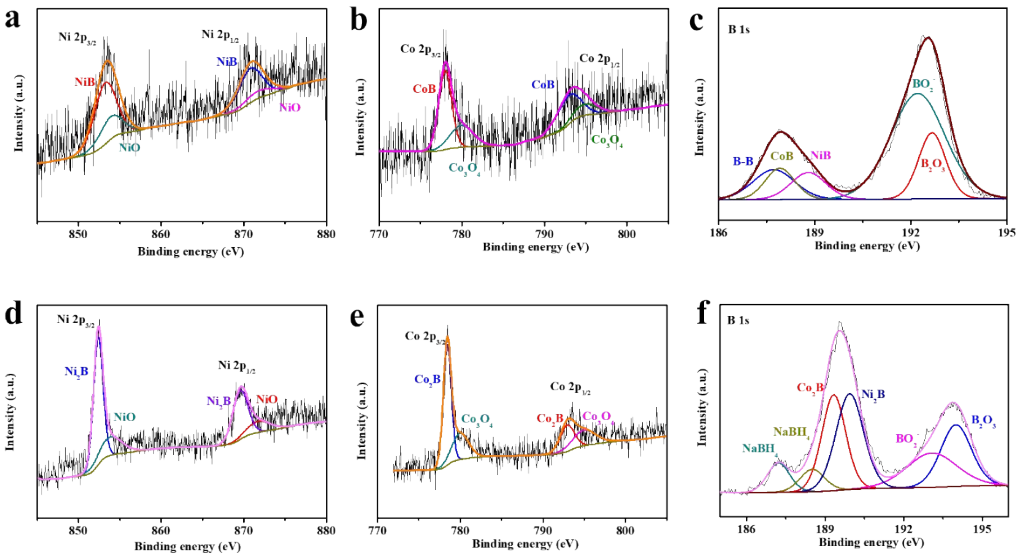

Figure S6. High-resolution Ni 2p, Co 2p, and B 1s XPS spectra of $NaBH_4$@NiCo-NC after the first cycle of dehydrogenation process (a, b, c) and the 2nd cycle of rehydrogenation process (d, e, f).

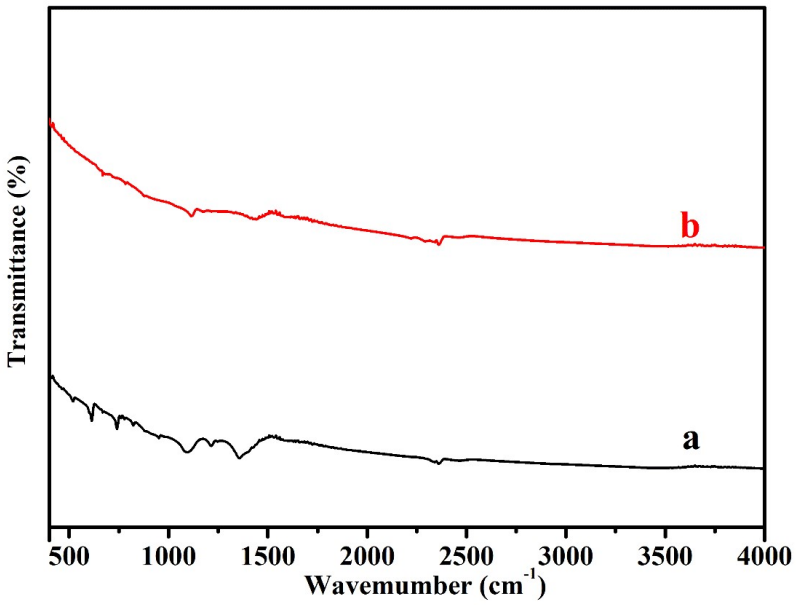

Figure S7. FTIR spectra of the dehydrogenation products of (a) $NaBH_4$/NiCo-NC and (b) $NaBH_4$@NiCo-NC.

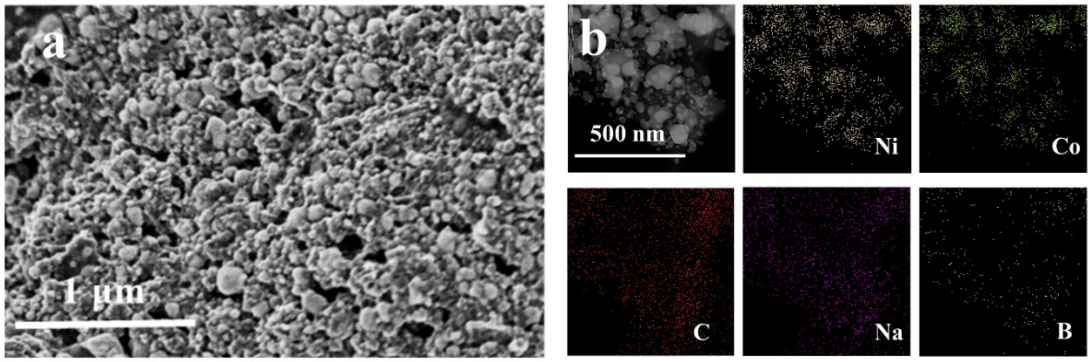

Figure S8. (a) SEM images and (b) STEM image and the corresponding EDS mapping of $NaBH_4$@NiCo-NC after the initial dehydrogenation process.

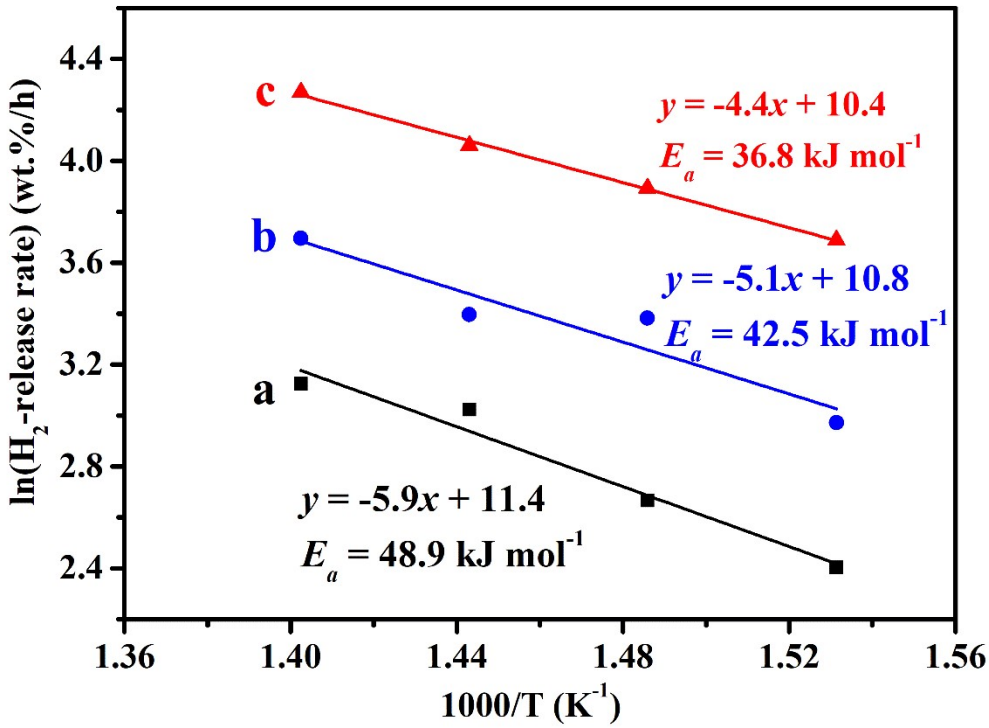

Figure S9. Arrhenius profiles of the dehydrogenation kinetics of (a) $NaBH_4$@NC, (b) $NaBH_4$/NiCo-NC, and (c) $NaBH_4$@NiCo-NC.

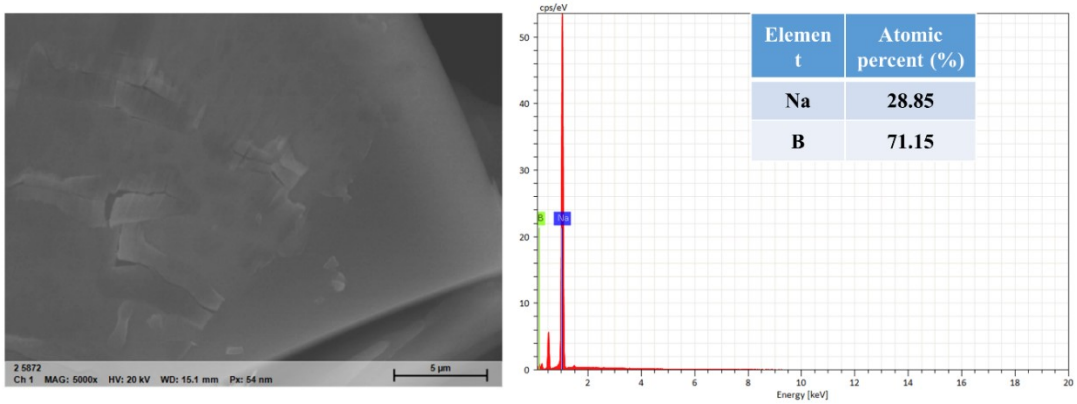

Figure S10. SEM image and the relative element content analysis of bulk $NaBH_4$ after the release of H_2 with a capacity of 9.0 wt.%.

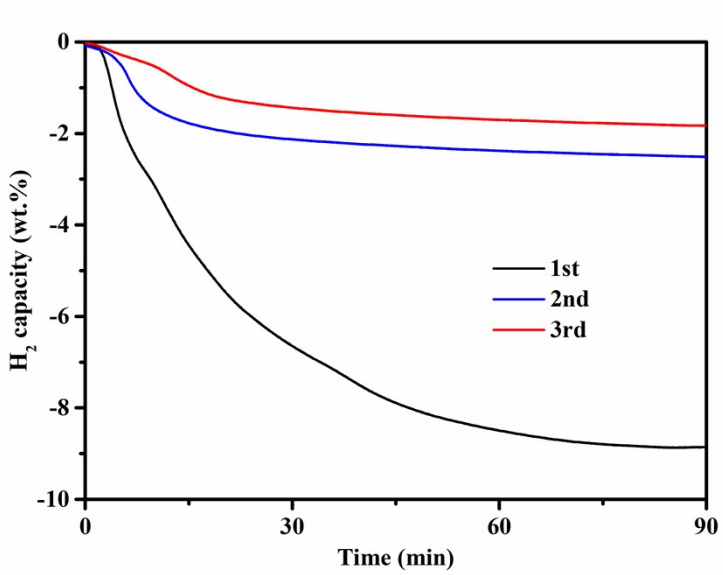

Figure S11. Cycling H_2 desorption performance of bulk $NaBH_4$ at 550 ℃.

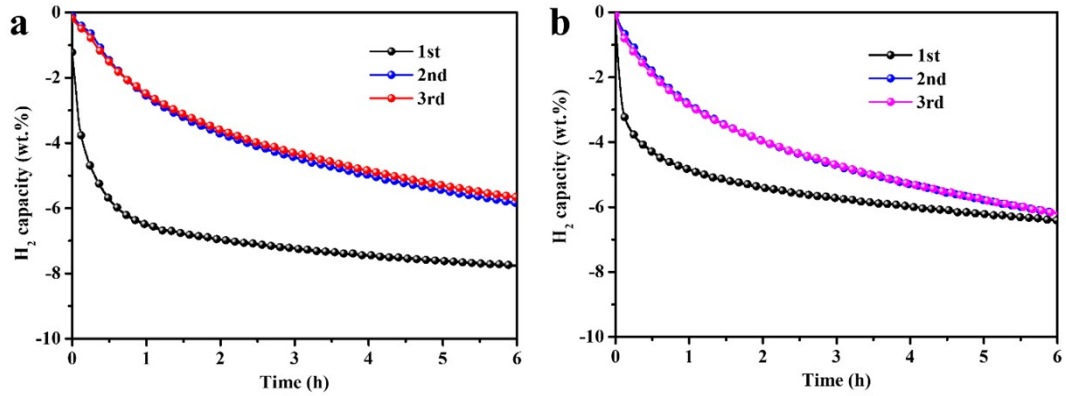

Figure S12. Cycling H_2 desorption performance of (a) $NaBH_4$/NiCo-NC and (b) $NaBH_4$@NC at 400 ℃.

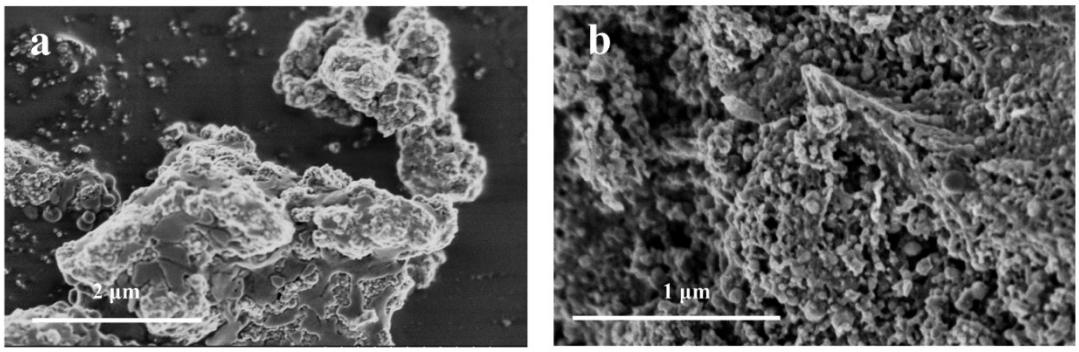

Figure S13. SEM images of the dehydrogenation product of (a) $NaBH_4$/NiCo-NC and (b) $NaBH_4$@NC.

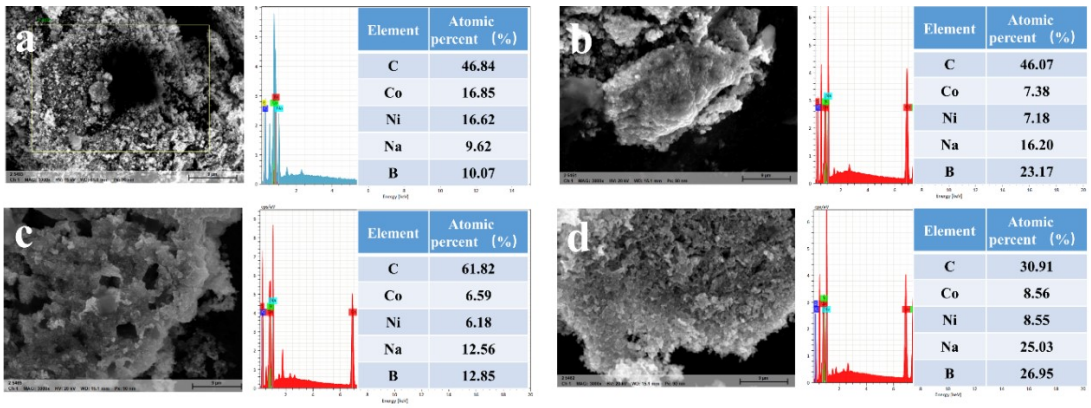

Figure S14. SEM images and the relative element content analysis of (a) $NaBH_4$/NiCo-NC, (c) $NaBH_4$@NiCo-NC and the dehydrogenation products of (b) $NaBH_4$@NiCo-NC, (d) $NaBH_4$/NiCo-NC.

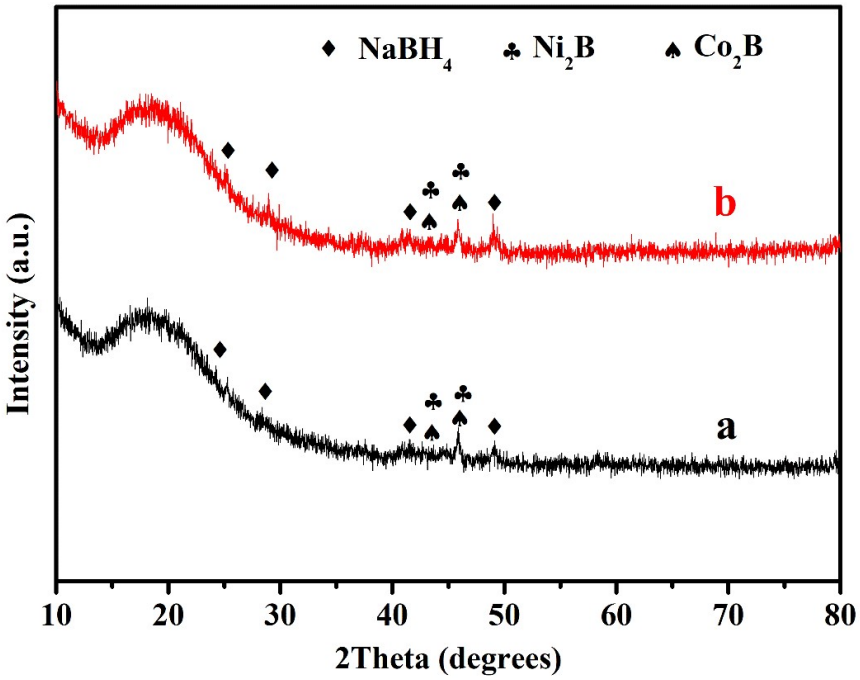

Figure S15. XRD patterns of the (a) $NaBH_4$/NiCo-NC and (b) $NaBH_4$@NiCo-NC after rehydrogenation.

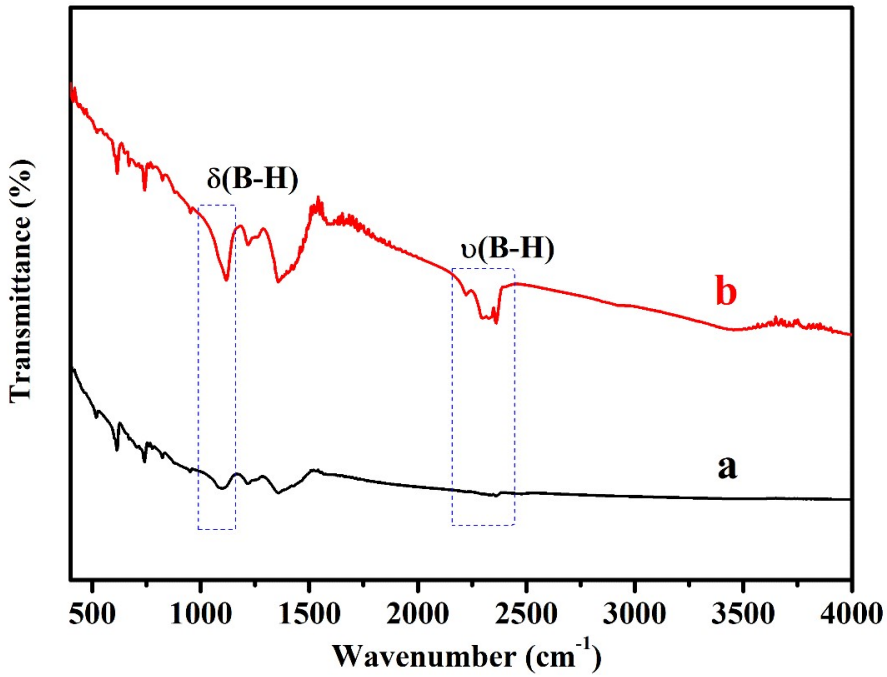

Figure S16. FTIR spectra of the (a) $NaBH_4$/NiCo-NC and (b) $NaBH_4$@NiCo-NC after rehydrogenation.

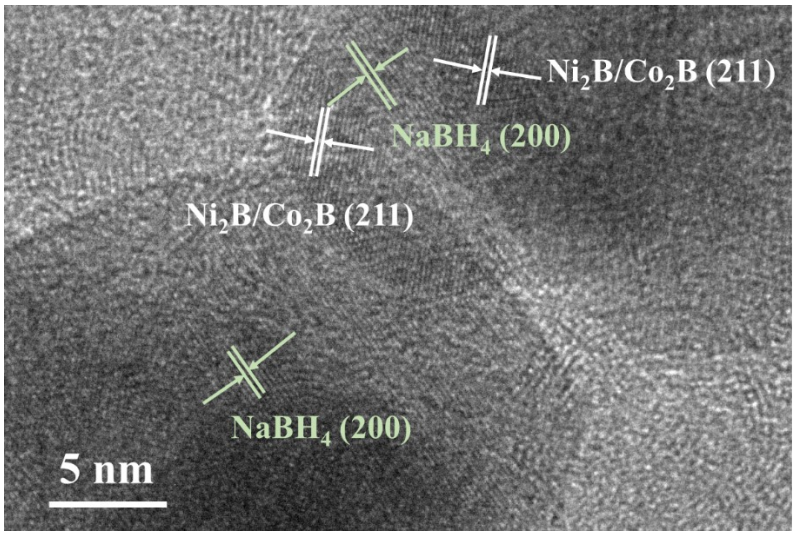

Figure S17 HRTEM image of $NaBH_4$@NiCo-NC after rehydrogenation.

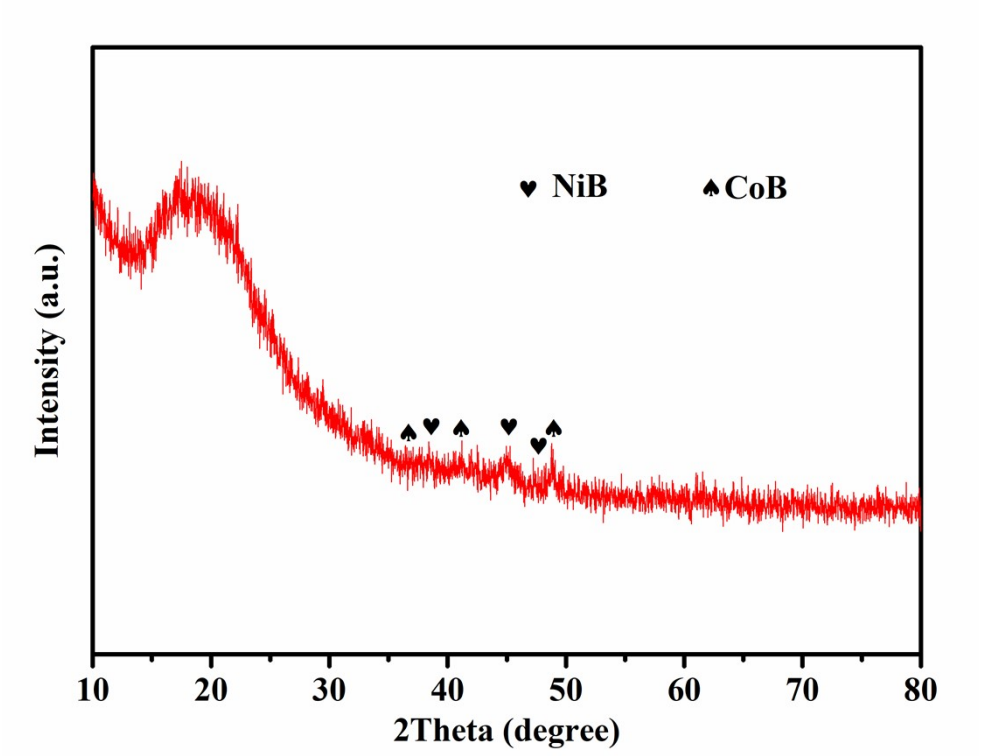

Figure S18. XRD patterns of $NaBH_4$@NiCo-NC after the 2nd dehydrogenation.

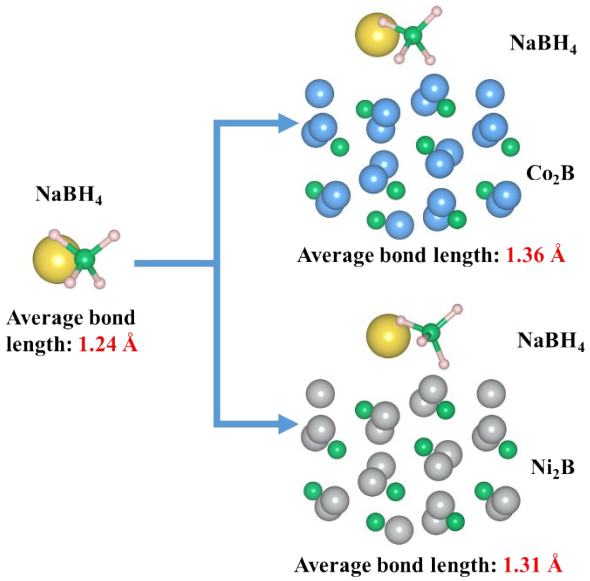

Figure S19. The optimized configurations of $NaBH_4$ molecule with and without the interaction of Co_2B/Ni_2B

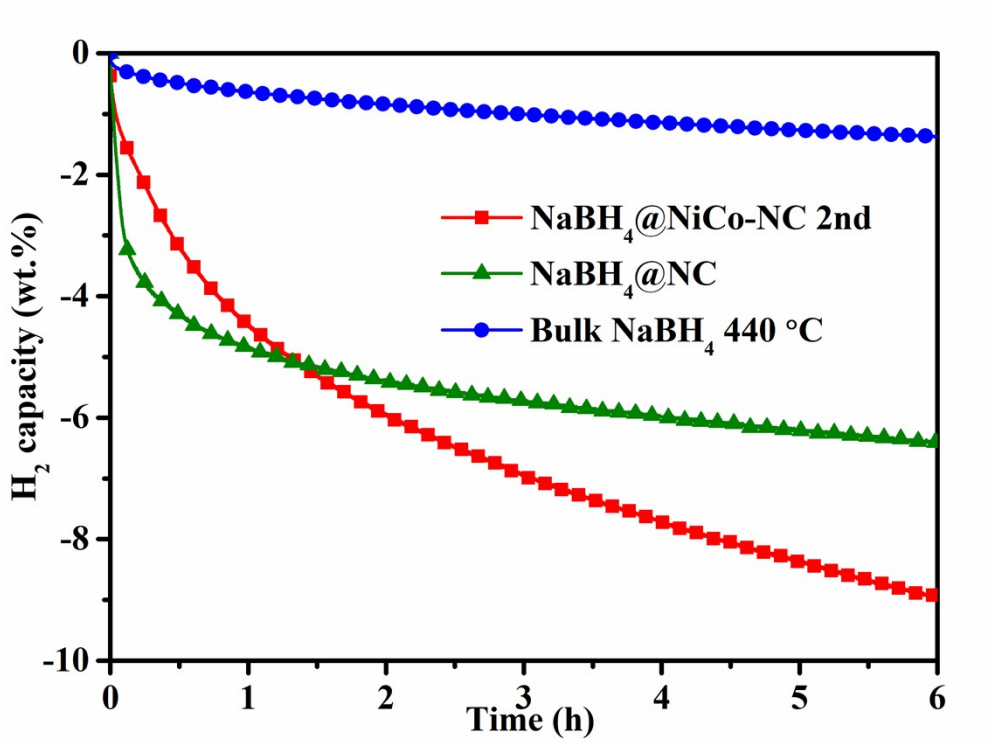

Figure S20. Isothermal H_2 desorption kinetics of $NaBH_4$@NiCo-NC for the 2nd cycle at 400 ℃, with the initial dehydrogenation kinetics of $NaBH_4$@NC at 400 ℃ and bulk $NaBH_4$ at 440 ℃ included for comparison.

Table S1. The comparison of hydrogen storage performance of various nanoconfined $NaBH_4$

Scaffolds	Peak temperature, ramping rate	Cycling performance	References
Nanoporous carbon	350 °C, 5 °C/min	43% of the initial capacity, 2 cycles	S8
Graphene	400 °C, 3 °C/min	~7.0 wt%, 6 cycles	S9
Ni coating	418 °C, 10 °C/min	~2.5 wt%, 5 cycles	S10
Co coating	450 °C, 10 °C/min	0.3 wt.%, 2cycles	S11
Fe coating	~460 °C, 10 °C/min	0.8 wt.%, 2cycles	S11
Cu coating	~460 °C, 10 °C/min	0.1 wt.%, 2cycles	S11
MCM-41	511 °C, 10 °C/min	——	S12
Mesoporous silica	400 °C, 2 °C/min	——	S13
NiCo-NC	356 °C, 3 °C/min	4.5 wt.%, 5 cycles	This work

References

S1 S. L. Zhao, Y. Wang, J. C. Dong, C.-T. He, H. J. Yin, P. An, K. Zhao, X. F. Zhang, C. Gao, L. J. Zhang, J. W. Lv, J. X. Wang, J. Q. Zhang, A. M. Khattak, N. A. Khan, Z. X. Wei, J. Zhang, S. Q. Liu, H. J. Zhao and Z. Y. Tang, *Nat. Energy*, 2016, **1**, 16184.

S2 Y. Z. Wang, Y. X. Liu, H. Q. Wang, W. Liu, Y. Li, J. F. Zhang, H. Hou and J. L. Yang, *ACS Appl. Energy Mater.*, 2019, **2**, 2063-2071.

S3 G. Kresse and J. Hafner, *Phys. Rev. B*, 1993, **47**, 558-561.

S4 G. Kresse and J. Furthmüller, *Phys. Rev. B*, 1996, **54**, 11169-11186.

S5 P. E. Blöchl, *Phys. Rev. B*, 1994, **50**, 17953-17979.

S6 J. P. Perdew, K. Burke and M. Ernzerhof, *Phys. Rev. Lett.*, 1996, **77**, 3865-3868.

S7 S. Grimme, J. Antony, S. Ehrlich and H. Krieg, *J. Chem. Phys.*, 2010, **132**, 154104.

S8 P. Ngene, R. V. D. Berg, M. H. W. Verkuijlen, K. P. de Jong and P. E. de Jongh, *Energ. Environ. Sci.*, 2011, 4, 4108-4115.

S9 L. N. Chong, X. Q. Zeng, W. J. Ding, D. J. Liu and J. X. Zou, *Adv. Mater.*, 2015, **27**, 5070–5074.

S10 M. L. Christian and K. F. Aguey-Zinsou, *ACS nano*, 2012, **6**: 7739-7751.

S11 M. L. Christian and K. F. Aguey-Zinsou, *Chem. Commun.*, 2013, **49**, 6794-6796.

S12 X. Luo, A. Rawal and K. F. Aguey-Zinsou, *Inorganics*, 2021; **9**:2.

S13 F. Perua, S. Garronia, R. Campesib, C. Milanesec, A. Marinic, E. Pellicerd, M. D. Baród and G. Mulas, *J. Alloys Compd.*, 2013, **580**, 309-312.